

Design and Performance of a W-Band MMW/IR Compound Cassegrain Antenna System with a Hyperbolic Sub-Reflector Based on Frequency Selective Surface

Min Han, Guo-Qiang Zhao*, Mang He,
Pei Zheng, Zhang-Feng Li, Cheng Jin, and Hou-Jun Sun

Abstract—A MMW/IR compound Cassegrain antenna system for mono-pulse radar applications is presented in this paper. By comparing different modeling methods of conformal frequency selective surface (CFSS), a sub-reflector, with a good performance of reflection at 93 GHz and transparency at the wavelength of 1.06 μm , is achieved according to sputtering technique. At the wavelength of 1.06 μm , transmittance of the sub-reflector is 67%. Compared to a Cassegrain antenna system consisting of a metallic sub-reflector with identical size, the gain of the compound antenna system has a negligible loss (less than 0.4 dB) at 93 GHz. Compared with the patent in [13], the design can improve the limited size of receiving system and the utilization of aperture of the compound detection system at IR region, and can also enhance the heat dissipation.

1. INTRODUCTION

In the target seeking systems of piloted aircrafts and guided missiles, millimeter wave (mm-wave) and infrared (IR) dual-mode sensors are typically used. The millimeter-wave (MMW) radar can operate under all weather conditions while the passive infrared (IR) sensor can provide much higher resolution [1]. Traditionally, the dual-mode sensors use curved reflectors to collect MMW and IR energy and focus them on appropriate detectors. To collect the maximum incoming energy and resolve problems triggered by limited aperture, a common aperture is usually employed.

Frequency selective surface (FSS) is a key technology to achieve common aperture sensor. FSS is a spatial filter, which consists of a periodic array of conductive patches or slots/apertures [2]. It can select signals with desired frequencies and has been widely used in hybrid radomes [3–5], dichroic sub-reflectors [6, 7], absorbers [8, 9], meander line polarizers [10], etc.

In the applications of common aperture, the period of FSS can only be finite, and the structure of FSS often is supposed to be conformal with work platform, such as tapered radome and hyperbolic main-reflector/sub-reflector. So the study of limited period curved FSS has a very practical value. As for its research, there are certain difficulties in the aspects of modeling, simulation, and processing, such as deformation of units, destruction of periodic structure and the missing shape of units on edge.

Currently, several processing methods of curved FSS have been studied. Planar method is usually adopted for singly-curved FSS (SCFSS), because its surface is folded into the singly-curved such as cylindrical or conical surfaces. Stamping [11] and paste methods [12] have been applied to doubly-curved FSS (DCFSS) design. By stamping method, the accuracy attainable is low, since the deformations cannot be controlled when the plane dichroic surface is pressed against a curved mold. The deformations

Received 30 August 2015, Accepted 9 November 2015, Scheduled 17 November 2015

* Corresponding author: Guo-Qiang Zhao (3120100284@bit.edu.cn).

The authors are with the Beijing Key Laboratory of Millimeter wave and Terahertz Technique, Beijing Institute of Technology, Beijing 100081, China.

depend on many factors difficult to control, such as the uniformity of thickness of curved face, and the uniformity of the stress. Paste method is described in [12]. According to this method, the dichroic structure is directly fabricated on the final curved structure by manually deposited planar units. Clearly, this method is not highly satisfactory because of the low accuracy and long time consumption.

To form a W-band/IR common aperture Cassegrain antenna system, comparing with different effects of DCFSS modeling methods, a FSS sub-reflector, which allows the signal with the wavelength of $1.06\ \mu\text{m}$ to pass and blocks the signal with the wavelength of $3.2\ \text{mm}$, is designed and fabricated according to sputtering technique with a curved metal mask. Compared with other methods, the higher accuracy of the adopted method is $\pm 0.01\ \text{mm}$. By replacing the traditional metallic sub-reflector, the measured results of the novel compound Cassegrain antenna system are in accordance with the simulated ones and meet the requirements of the compound system. Compared with the patent [13], the heat dissipation problem is solved and IR utilization improved.

2. HYPERBOLICALLY CONFORMAL FSS

The hyperbolically conformal FSS studied in this paper has to satisfy the following requirements. Firstly, it should be insensitive to the incident angle and polarization of the detected signals. Secondly, it should be transparent to IR signals while reflective to MMW signals. Thirdly, it should possess the same geometric optical property as the traditional hyperbolic sub-reflector. As a result, modeling conformal methods and selection parameters for FSS cell will be analyzed and optimized to meet such requirements.

2.1. Modeling Conformal Methods

Modeling and analysis of conformal FSS (CFSS) is particularly important when FSS is used for reflectors/sub-reflectors or radomes. To the DCFSS, local planarization [14] and normal projection method [15] have been widely applied. The first one is used only when the periodicity of the gratings is considerably smaller than the minimum radius of curvature, while discontinuity of adjacent parts, deformation and destruction of periodicity are the main problems encountered in the second method.

To solve the problems mentioned above, normal projection and two other different projection methods for arbitrary curved FSS are illustrated and compared in details. In this part, the direction of the curved surface symmetry is z -axis, and the tangent plane over the vertex is xoy plane.

2.1.1. Normal Projection Method

Figure 1(b) shows the principle of the normal projection (NP) method, which is along with the normal direction of the curved surface. A planar FSS is placed upon the curved surface and paralleled to xoy plane. Along with the normal direction of the curved surface, the projection is made by the rays which pass through the edges of unit cells.

However, this method will bring the curved FSS unit different degrees of distortion. And the longer the distance is from the center of the surface, the larger the distortion degree becomes.

2.1.2. Vertical Projection Method

The vertical projection (VP) method is shown in Fig. 1(c). The dotted lines describe the vertical projected direction which is along the z -axis. When the curvature of the curved surface is large enough, the projection error should not be neglected. The CFSS unit distortions are enlarged with the increased distance from the center of the curved surface. If the curved surface is electrically large, the distortion of projection can be neglected.

2.1.3. Modified Vertical Projection Method

In order to reduce the distortion caused by the vertical projection, a modified vertical projection (MVP) method is shown in Fig. 1(d). O_1 and O_3 are the centers of unit 1 and unit 3, respectively, and $O_{1'}$, $O_{3'}$ are the vertical projection of O_1 , O_3 . Units $1'$, $3'$ are parallel to the tangent plane of the curved surface. The projections of these units are obtained by the rays whose direction is along z -axis. Compared

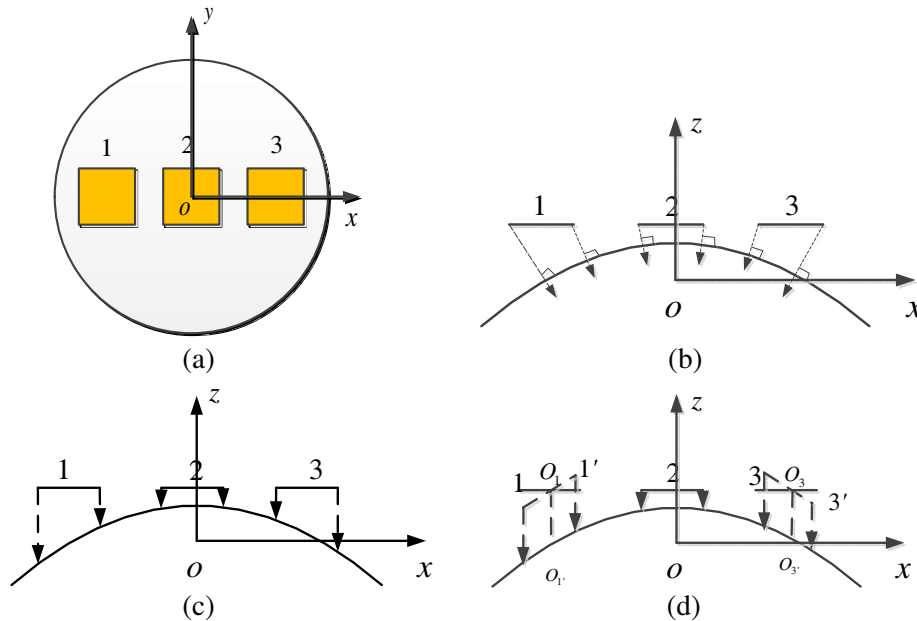


Figure 1. Projection methods. (a) Top view. (b) Side view of normal projection (NP). (c) Vertical projection (VP). (d) Modified vertical projection (MVP).

with the direct projection method mentioned before, this method has smaller distortion but is more time-consuming.

2.2. Selection of Parameters for FSS Cell and Sub-Reflector

Consider the printed dipole units shown in Fig. 2. The surface is periodic and is assumed to be infinite in xy plane. The crossed dipole, insensitive to the polarization of the incident signals [11], is chosen. Polycarbonate, used as the substrate, of which the thickness is 1 mm with the loss tangent of 0.008 and the relative permittivity of 2.7, is transparent to IR signals. The optimization object is to get a reflection coefficient close to 0 dB across a wide frequency band centered at 93 GHz. The final optimized parameters are listed in Table 1.

Table 1. Optimized parameters.

Symbol	p/mm	l/mm	w/mm	h/mm	r/mm
Quantity	1.40	1.27	0.13	1.00	0.05

Using full wave simulator, ANSYS HFSS, the reflection coefficient’s magnitude is shown in Fig. 2(b). Evidently, the resonant frequency is very stable with respect to the incident angle variation. With incident angles from normal to 45° , the absolute maximum discrepancy of reflection coefficient is about 0.005 dB. All the results demonstrate that the cross dipole element is insensitive to both polarization and incident angles.

Figure 3 shows three 2.4-cm diameter hyperbolic sub-reflectors of design (eccentricity = 2.24) with the same parameters and different projection methods described in the previous section. The three models are similar in macro view but are different in terms of number units, with 241, 221 and 221, respectively. And metal areas are 49.58, 54.82 and 50.08 mm^2 , respectively.

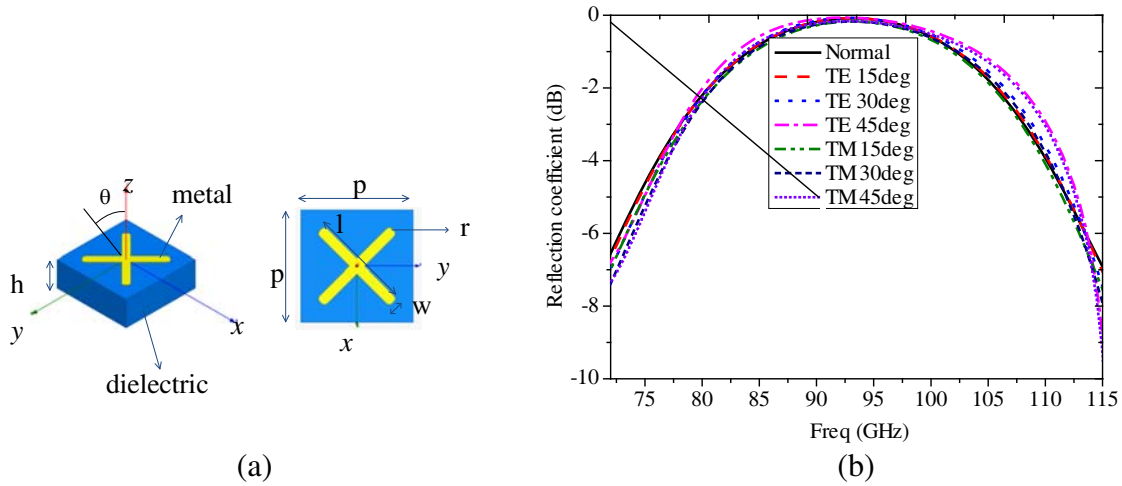


Figure 2. Unit cell shapes and its frequency response. (a) Unit cell. (b) Reflection parameters with different polarizations and incident angles.

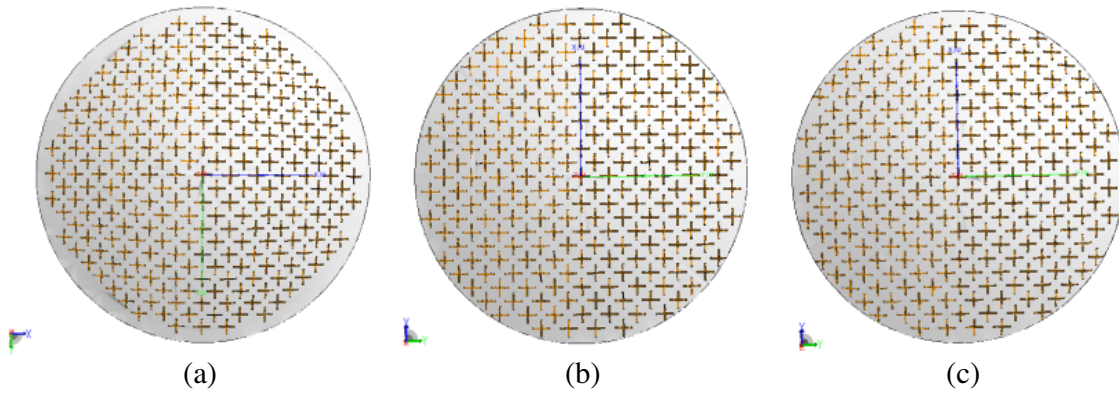


Figure 3. Different projected FSS models. (a) NP-FSS. (b) VP-FSS. (c) MVP-FSS.

2.3. Simulated Results

Figure 4(a) shows the scheme of simulation for reflection of designed FSS models. One double-ridge horn, operated from 80 GHz to 105 GHz with its dimensions of $12\text{ mm} \times 15\text{ mm} \times 28.4\text{ mm}$, is placed to one side of an FSS at a distance R , which is the near-field range of the antenna. To evaluate its reflection performance, a metal model with the same parameters is used for comparison. Fig. 4(b) shows the simulated reflection coefficient. The physical distance between the horn and the center of the curved face is 5.5 mm which is about $1.7\lambda_0$. Evidently, the FSS simulated results are in close agreement with the metal one. There is, however, a slight difference between them which may be attributed to the dielectric loss. In addition, from 90 to 101 GHz, it is seen that the reflection coefficient of MVP is a little better than VP. But all of the FSSs can successfully provide good stop-band property, which indicates that projection methods are feasible. Thus, the fact that the different models obtain similar results can prove the feasibility of these projection methods. In addition, it also indicates the possibility of reducing the difficulty of processing in the perspective of engineering application.

For the size of the FSS unit (1.27 mm) is larger than the wavelength of IR ($1.06\ \mu\text{m}$), the transmitted performance of IR can be calculated using the equation in [16]. Non-metallic and whole areas of the sub-reflector are 421.93 mm^2 and 476.75 mm^2 , respectively. Therefore, the theoretical effective transmittance is calculated to be 88.5%.

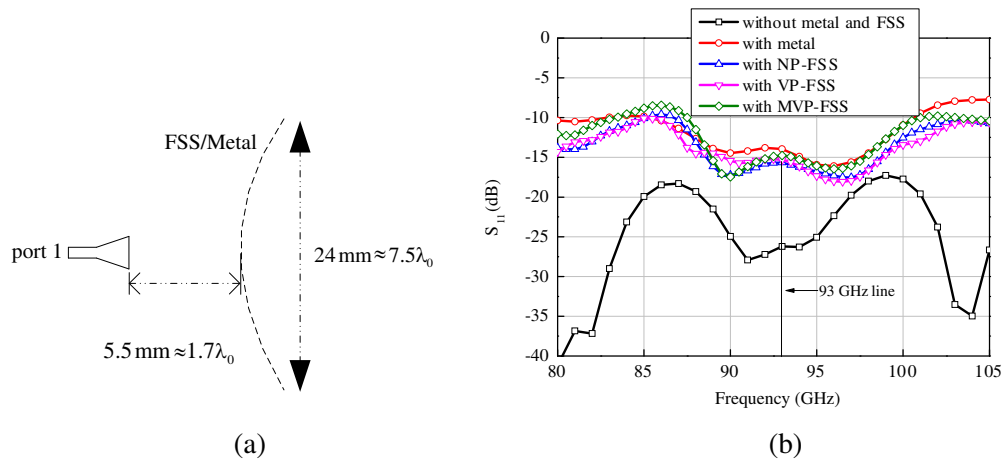


Figure 4. Simulation system of reflection coefficient. (a) Model. (b) Reflection coefficient using full wave simulator HFSS.

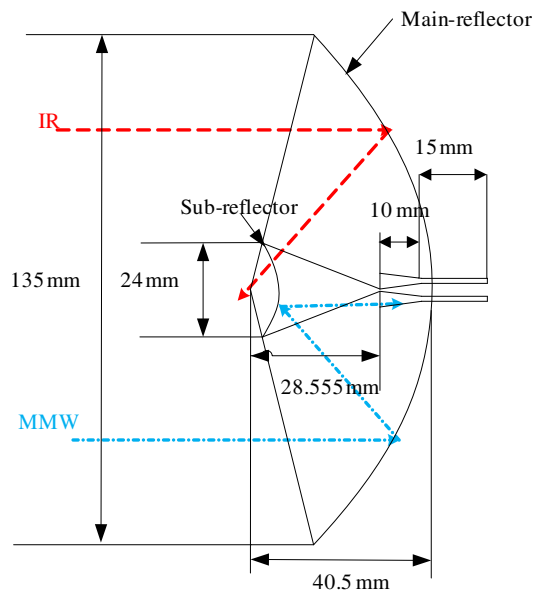


Figure 5. Parameters of Cassegrain antenna.

3. FABRICATIONS AND MEASUREMENTS

Figure 5 shows a 13.5-cm parabolic dish ($f/D = 0.3$) in the Cassegrain mode. The feed horns is located at the focus of the main reflector, and the inner dimension is 4.5 mm (E -plane) \times 4.7 mm (H -plane). The flare angles are 18.4 and 19.2 degrees, respectively.

3.1. Fabrication of the Sub-Reflector

Using the parameters of Fig. 2(b), a metal mask, shown in Fig. 6, is made by electric discharging machining technology by a computer program. The mask is used for sputtering metal on a 1-mm polycarbonate sheet. Compared with pressed against mold method [11], sputtering method can improve precision especially on high-frequency application.

With the same parameters of VP model, the final product is shown in Figs. 6(d), (e). The surface is metalized with platinum complicated by sputtering process, with a thickness about 1 μ m. This sub-reflector weighs about 20 g and has a surface accuracy of + or -0.01 mm.

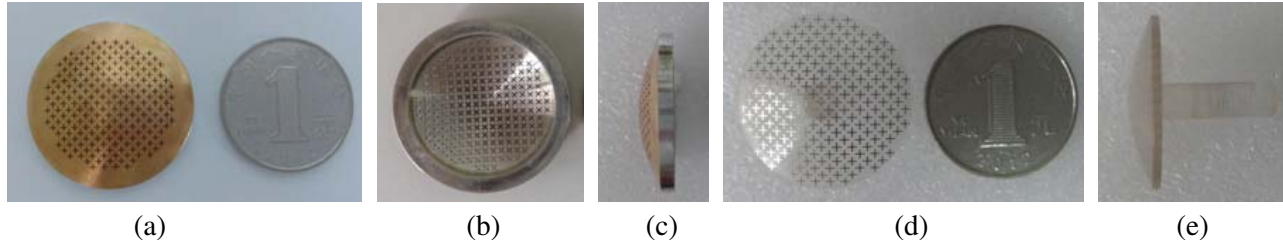


Figure 6. Photos of the fabricated mask and subreflector. (a) Top view, (b) back view, (c) side view of metal mask. (d) Top view, (e) side view of sub-reflector.



Figure 7. Photos of fabricated Cassegrain antenna.

3.2. Performance Evaluation

All measurements are taken as receiving patterns on a 10-m antenna range. Fig. 7 shows the assembled Cassegrain antenna system. Firstly, the metallic sub-reflector is mounted, and its position is axially and longitudinally adjusted to obtain a focused pattern with sharp nulls. The sub-reflector is then removed, and the FSS one is replaced. These positions of the two sub-reflectors are maintained throughout the measurements. Patterns are recorded in such a way that the FSS sub-reflector is positioned exactly where the front metallic one should have been.

Typical patterns recorded with two sub-reflectors are shown in Fig. 8. The simulation method used in Fig. 8 is FEKO 6.0, and the used algorithm is a mixture of physical optics (PO) and multilevel fast multipole (MLFMM). The two patterns, namely those respectively measured with metallic and FSS sub-reflector results at 93 GHz, have the shape of the main beam at least up to 15 dB below the peak. Also a comparison of the measured and simulated results in each of the two patterns are shown in Table 1. The measured 3 dB beam-width of FSS sub-reflector is 2.12–2.13 degree, and the first sidelobe level is about -17.5 dB. The double peak unevenness is below 1.6 dB. One possible reason for this discrepancy phenomenon can be attributed to asymmetric fixed struts shown in Fig. 7. The small difference in the measured and simulated results may be attributed to the fabrication tolerances and measured errors.

Maybe because of the dielectric loss or the reflected loss of FSS, the measured gain of FSS is a little lower than PEC. In Fig. 2(b), the simulated reflected parameter (S_{11}) is -0.11 dB at 93 GHz. The measured gain of metallic sub-reflector antenna is superior to the simulated one maybe for its narrower width, which is 1.50 dB (E -plane) and 1.52 dB (H -plane) less than the simulated one 1.88 dB (E -plane) and 2.18 dB (H -plane).

The transmittance from the wavelength of $0.25 \mu\text{m}$ to $1.10 \mu\text{m}$ can be measured by an ultraviolet and visible spectro-photometer SHIMAZU 3600. In Fig. 8, it is presented that the transmittance of the designed FSS is 67% at $1.06 \mu\text{m}$. The measured transmittance result (66.7%) is lower than the theoretical effective transmittance (88.5%). But compared with the patent in [13], the high utilization of the antenna aperture in this band can compensate for the loss caused by the media. Evidently the FSS sub-reflector meets all the requirements set for the design.

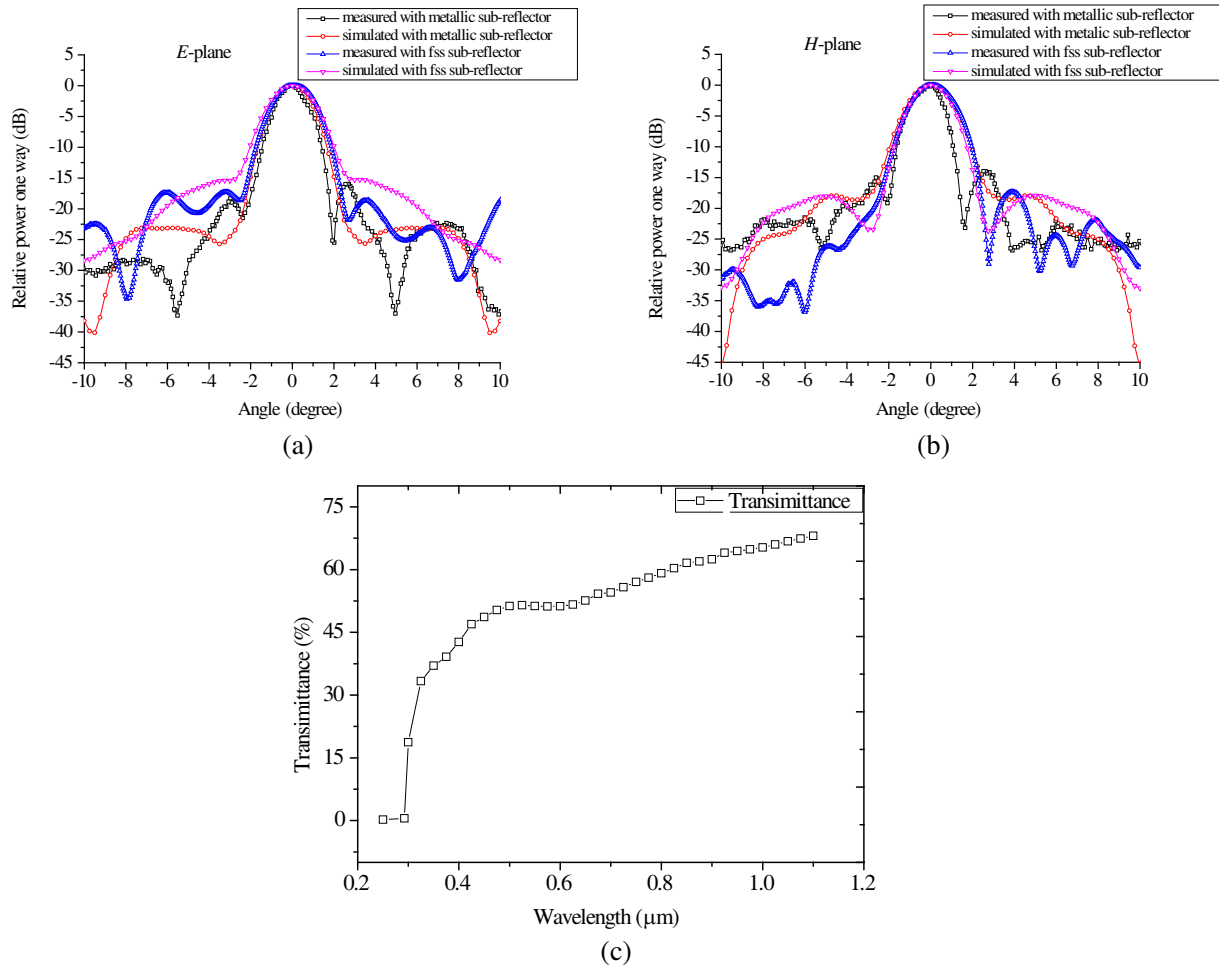


Figure 8. Measured Results. (a) Radiation patterns of the antenna at 93 GHz of *E* plane and (b) *H* plane. (c) Sub-reflector transmittance of IR.

4. CONCLUSION

Based on different modeling methods of projection CFSS, a hyperbolical FSS, with transparent performance to the signals at IR band and reflected at MMW band, is designed for Cassegrain antenna applications. The main process is to project a plane FSS on the surface of a hyperboloid and fabricate on a substrate of polycarbonate. The measured results of the Cassegrain antenna with the designed FSS sub-reflector agree well with the simulation. The gain is 34.54 dB at 93 GHz, and the transmittance at 1.06 μm is 67%. The performance of the designed FSS sub-reflector is close to the metallic sub-reflector systems with smaller size and better heat dissipation. It also improves the utilization of aperture in the complex detection system of patent [13].

REFERENCES

1. Klein, L. A., *Millimeter Wave and Infrared Multisensor Design and Signal Processing*, 1–47, Artech House, Boston, 1997.
2. Munk, B. A., *Frequency Selective Surfaces: Theory and Design*, 1–21, John Wiley Interscience, New York, 2000.
3. Hang, Z., S. Qu, B. Lin, et al., “Filter-antenna consisting of conical FSS radome and monopole antenna,” *IEEE Antennas and Wireless Propagation Letters*, Vol. 60, No. 6, 3040–3045, 2012.

4. Chen, H., X. Hou, and L. Deng, "Design of frequency-selective surfaces radome for a planar slotted waveguide antenna," *IEEE Antennas and Wireless Propagation Letters*, Vol. 8, 1231–1233, 2009.
5. Gustafsson, M., "RCS reduction of integrated antenna arrays and radomes with resistive sheets," *IEEE Antennas and Propagation Society International Symposium*, 3479–3482, Albuquerque NM, 2006.
6. Bresciani, D., S. Contu, C. Bruno, et al., "Design of a 1 m dichroic subreflector for K and Ku frequency bands," *IEEE Antennas and Propagation Society International Symposium*, 1084–1087, San Jose, CA, USA, 1989.
7. Lima, A. D. C. and E. Parker, "Fabry-Perot approach to the design of double layer FSS," *IEE Proceedings-Microwaves Antennas and Propagation*, Vol. 143, No. 2, 157–162, 1996.
8. Kiani, G. I., K. L. Ford, K. P. Esselle, et al., "Oblique incidence performance of a novel frequency selective surface absorber," *IEEE Transactions on Antennas and Propagation*, Vol. 55, No. 10, 2931–2934, 2007.
9. Costa, F. and A. Monorchio, "A frequency selective radome with wideband absorbing properties," *IEEE Transactions on Antennas and Propagation*, Vol. 60, No. 6, 2740–2747, 2012.
10. Euler, M., V. Fusco, R. Cahill, et al., "325 GHz single layer sub-millimeter wave FSS based split slot ring linear to circular polarization convertor," *IEEE Transactions on Antennas and Propagation*, Vol. 58, No. 7, 2457–2459, 2010.
11. Agrawal, V. D., "Design of a dichroic Cassegrain subreflector," *IEEE Transactions on Antennas and Propagation*, Vol. 27, No. 4, 466–473, 1979.
12. Zhang, C., X.-L. Liu, Q. Yang, et al., "Research of airborne radomes curved FSS array graphics," *Production Technology Branch of China Electronic Institute Electricity Processing Professional Committee of the Sixth Academic Essays*, 224–227, 2000.
13. Sanders, R. J., J. D. Shmoldas, and D. A. Wicks, "Dual-frequency millimeter wave and laser radiation receiver," US, 6268822.2001-07-03, <http://www.freepatentsonline.com/6268822.pdf>.
14. Hou, X.-Y., P. Zhang, and J. Lu, "A novel frequency selective design for double curved radome," *Journal of Projectiles, Rockets, Missiles and Guidance*, Vol. 26, 123–125, 2006.
15. Cui, X., "Analysis and simulation of the bandpass radome application based on FSS," Master Dissertation in Northwestern Polytechnical University, 2006.
16. Bhattacharyya, A. K., *High-frequency Techniques: Recent Advance and Applications*, 261, New York, USA, John Wiley Interscience, 1995.